*J. King Saud Univ.*, Vol. 9, *Eng. Sci.* (2), pp 265-293 (A.H. 1417/1997)

# Numerical Solution of Periodic Heat Transfer in an Anisotropic Cylinder Subject to Asymmetric Temperature Distribution

**Bassam A. Abu-Hijleh**
*Mechanical Engineering Department, Jordan University of Science and Technology*
*P.O. Box 3030, Irbid 22110, Jordan*

(Received 30 October 1995; accepted for publication 28 September 1996)

**Abstract.** This paper details the numerical solution of the heat conduction problem in a two-dimensional anisotropic cylinder subject to asymmetric and periodic temperature distribution on the outer wall. The dimensional analysis of the problem reveals that the heat conduction is a function of five non-dimensional parameters. The parameters are: non-dimensional frequency ($\alpha$), cylinder outer to inner radius ratio ($R_2$), Biot number (Bi), orthotropicity factor ($K_{22}$), and anisotropicity factor ($K_{12}$). The study details the effect of each parameter on the maximum radial heat conduction to the cylinder inner and outer walls, $q_1$ and $q_2$ respectively, as well as the phase shift between $q_1$ and $q_2$. Depending on the combination of the parameters, the magnitude and/or phase of heat conduction in an anisotropic cylinder can be significantly different from those of an orthotropic and isotropic cylinder subject to the same externally imposed temperature distribution.

## Nomenclature

| | | |
|---|---|---|
| Bi | = | Biot number, $Bi = h\, r_1 / k_{11}$ |
| $C_p$ | = | Specific heat of cylinder material |
| h | = | Convection heat transfer coefficient |
| $K_{ij}$ | = | Non-dimensional cross direction conduction coefficient |
| $K^*_{12}$ | = | Non-dimensional cross direction conduction coefficient normalized using $K_{22}$ |
| $k_{ij}$ | = | Cross direction conduction coefficient |
| m | = | Number of nodes in the tangential direction |
| n | = | Number of nodes in the radial direction |

| | | |
|---|---|---|
| $Q$ | = | Maximum magnitude of dimensional radial heat conduction irrespective of tangential location; $Q(r)$ |
| $q$ | = | Maximum magnitude of the non-dimensional radial heat conduction irrespective of tangential location; $q(R) = \max [q_L(R,\theta) \; \forall \; \theta)]$ |
| $q_L$ | = | Local non-dimensional radial heat conduction; $q_L(R, \theta)$ |
| $R$ | = | Non-dimensional radius, $R = r / r_1$ |
| $r$ | = | Radius |
| $T$ | = | Temperature |
| $T_{avg}$ | = | Average value of imposed temperature on cylinder outer surface |
| $T_o$ | = | Coefficient in the fluctuating temperature distribution of the cylinder outer surface |
| $T_\infty$ | = | Temperature at which convection occurs at the cylinder inner radius |
| $t$ | = | Time |

**Greek symbols**

| | | |
|---|---|---|
| $\alpha$ | = | Non-dimensional frequency, $\alpha = \rho \, C_p \, \omega \, r_1^2 / k_{11}$ |
| $\gamma$ | = | Non-dimensional time |
| $\varepsilon$ | = | Tolerance parameter used to test for numerical convergence |
| $\zeta$ | = | Auxiliary non-dimensional temperature |
| $\xi$ | = | Spatial part of the complex non-dimensional temperature |
| $\theta$ | = | Tangential angle |
| $\rho$ | = | Density of cylinder material |
| $\phi$ | = | Non-dimensional temperature |
| $\psi$ | = | Complex non-dimensional temperature |
| $\omega$ | = | Frequency of imposed periodic heat flux. |

**Subscripts**

| | | |
|---|---|---|
| 1 | = | Relates to cylinder inner radius |
| 2 | = | Relates to cylinder outer radius |
| 11 | = | Radial direction |
| 12 | = | Cross term between radial and tangential directions |
| 22 | = | Tangential direction |

## Introduction

Several materials exhibit thermal anisotropic behavior. These include natural materials such as wood, crystals, and sedimentary rocks. More important is the anisotropic behavior of composite materials and alloys made using uni-directional crystal solidification techniques. Interest in anisotropic materials dates back to the late nineteenth and early twentieth centuries. Earlier work in this field focused on one-dimensional heat conduction in crystals [1,2]. Carslaw and Jaeger [3] discussed the general anisotropic heat conduction problem with emphasis on orthotropic materials. Analytical solutions to unsteady

anisotropic heat conduction problems relied on the use of Green's function but still proved extremely difficult [4].

With the increased use of composite materials in all engineering applications, the study of the effect of the anisotropic nature of such materials became more critical. Still researchers tended to concentrate their work on isotropic materials due in part to their predominant use. Researchers also tended to shy away from tackling anisotropic problems due to their more involved and complex mathematical nature. The analytical solution of a fully anisotropic problem is extremely difficult due to the cross direction conduction coefficient, $k_{ij}$.

The use of composite materials has increased exponentially in the last two decades. The main advantage of composite materials is the ability to tailor its properties as needed. For the most part, engineers are interested in the mechanical properties of composite materials to achieve the required tensile strength and bending moment characteristics. But tailoring the thermal properties of composite materials could prove as important when used as insulation materials. The diference in conduction coefficients beween the different directions can also give rise to uneven material expansion and contraction. This gives rise to what is known as thermal stresses [5].

Such stresses add to the stresses imposed by external loads and could result in failure if not taken into account. Such a situation will be encountered in the proposed space station which will be fabricated mainly using composite materials. The uneven and periodic exposure of the station's outer surface to the sun could be modeled by the problem presented herein. The same situation can also be encountered in several other situations on earth where structures made from composite materials are exposed to uneven heat energy sources. To the best of the author's knowledge, all recent papers relevant to this field dealt with either steady [6-10] or transient [11-15] heat transfer. Most of these papers focused on orthotropic materials [6,10-15] with little work on anisotropic materials [7-9]. A recent paper by the author presented an analytical solution of periodic heat transfer across an orthotropic cylinder [16]. The analytical solution is used to validate the accuracy of the numerical solution presented herein.

This paper will discuss the effect of five parameters on the heat conduction and phase shift in a two dimensional anisotropic cylinder subject to a steady periodic and asymmetric temperature distribution. It is of great importance to be able to determine the amount of heat being conducted to the cylinder inner wall under different conditions. As will the results show, a cylinder with high degree of orthotropicity exhibits superior insulation characteristics compared to an isotropic cylinder of similar dimensions. A cylinder with high degree of anisotropicity exhibits high and relatively constant radial heat conduction to the inner wall regardless of the imposed conditions. The phase shift is important when designing a measurement and/or feedback control system where such a cylinder is used

as a by-product of the solution, the time dependent temperature distribution is calculated across the cylinder. This can be used to study the thermal fatigue problem due to the dynamic thermal stresses in an anisotropic cylinder subject to an asymmetric and cyclic imposed temperature distribution.

## Mathematical Model

Figure 1 shows a schematic of the cylinder physical parameters as well as the imposed temperature and convective boundary conditions. The two dimensional unsteady heat conduction equation in an anisotropic cylinder can be written as follows [17]:

$$\rho C_\rho \frac{\partial T}{\partial t} = k_{11} \frac{1}{r} \frac{\partial}{\partial r}\left( r \frac{\partial T}{\partial r} \right) + 2k_{12} \frac{1}{r} \frac{\partial^2 T}{\partial r \partial \theta} + k_{22} \frac{1}{r^2} \frac{\partial^2 T}{\partial \theta^2} \qquad (1)$$

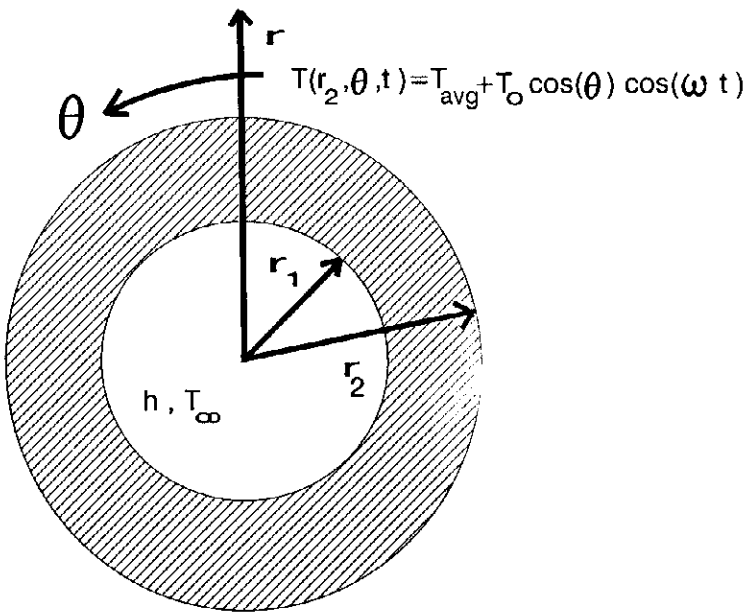


**Fig. 1. Schematic of the cylinder and boundary conditions.**

The equation will be solved in conjunction with the following boundary conditions:

$$k_{11}\frac{\partial T(r_1,\theta,t)}{\partial r}+k_{12}\frac{1}{r_1}\frac{\partial T(r_1,\theta,t)}{\partial \theta}=h[T(r_1,\theta,t)-T_\infty] \tag{2}$$

$$T(r_2,\theta,t)=T_{avg}+T_o\cos(\theta)\cos(\omega t) \tag{3}$$

$$T(r,\theta,t)=T(r,\theta+2\pi,t) \tag{4}$$

Since we are looking for the steady state periodic temperature distribution, no initial condition is required. This point will become evident later on in the derivation.

To simplify the analysis, define the following non-dimensional groups:

$$R\equiv\frac{r}{r_1}$$

$$\phi(R,\theta,\gamma)\equiv\frac{T\left(\frac{r}{r_1},\theta,\omega*t\right)}{T_o}$$

$$\gamma\equiv\omega t$$

$$K_{12}\equiv\frac{k_{12}}{k_{11}}$$

$$q_{periodic}(R,\theta,\gamma)=\frac{Q\left(\frac{r}{r_1},\theta,\omega*t\right)}{\frac{k_{11}T_o}{r_1}}$$

$$K_{22}\equiv\frac{k_{22}}{k_{11}}$$

$$Bi\equiv\frac{hr_1}{k_{11}}$$

$$\alpha\equiv\frac{\rho C_p\omega(r_1)^2}{k_{11}}$$

Using these groups, Eq. (1) can be rewritten as:

$$\frac{1}{R}\frac{\partial}{\partial R}\left(R\frac{\partial\phi}{\partial R}\right)+2K_{12}\frac{1}{R}\frac{\partial^2\phi}{\partial R\partial\theta}+K_{22}\frac{1}{R^2}\frac{\partial^2\phi}{\partial\phi^2}=\alpha\frac{\partial\phi}{\partial\gamma} \tag{5}$$

The focus of this work is on the periodic heat conduction through the cylinder. Thus the values of $T_{avg}$ and $T_\infty$ were set to zero. These comprise the DC component of the heat conduction. Their effect can easily be incorporated using superposition. Equations 2 and 3 can now be written, respectively, as:

$$\frac{\partial\phi(1,\theta,\gamma)}{\partial R}+K_{12}\frac{\partial\phi(1,\theta,\gamma)}{\partial\theta}=Bi\phi(1,\theta,\gamma) \tag{6}$$

$$\phi(R_2,\theta,\gamma)=\cos(\theta)\cos(\gamma);R_2\equiv\frac{r_2}{r_1} \tag{7}$$

The insulation effect of the symmetry plane passing through $\theta = 0$ and $\theta = \pi$ can be used to replace Eq. (4) as the boundary conditions in the tangential direction. The new conditions can be written as follows:

$$\frac{\partial\phi(R,\theta,\gamma)}{\partial\theta}=0 \tag{8}$$

$$\frac{\partial\phi(R,\pi,\gamma)}{\partial\theta}=0 \tag{9}$$

The solution of $\phi$ (R, $\theta$, $\gamma$) can be found indirectly by defining an auxiliary problem $\zeta$ (R, $\theta$, $\gamma$). The two problems are then combined to form a complex heat conduction problem $\psi$ (R, $\theta$, $\gamma$) as follows:

$$\psi(R,\theta,\gamma)=\phi(R,\theta,\gamma)+i\zeta(R,\theta,\gamma);i\equiv\sqrt{-1} \tag{10}$$

The solution required, $\phi$ (R, $\theta$, $\gamma$), is just the real part of $\psi$ (R, $\theta$, $\gamma$). The solution $\psi$ (R, $\theta$, $\gamma$) can be written as:

$$\psi(R,\theta,\gamma)=\xi(R,\theta)\exp(i\gamma) \tag{11}$$

The exp (i $\gamma$) term satisfies the periodic time condition without the need for an initial condition. After some mathematical manipulation, the governing equation for the complex heat condition problem can be written as:

$$\frac{1}{R}\frac{\partial}{\partial R}\left(R\frac{\partial\xi}{\partial R}\right)+2K_{12}\frac{1}{R}\frac{\partial^2\xi}{\partial R\partial\theta}+K_{22}\frac{1}{R^2}\frac{\partial^2\xi}{\partial\theta^2}=i\alpha\xi \tag{12}$$

Equation (12) is subject to the following boundary conditions:

$$\frac{\partial\xi(1,\theta)}{\partial R}+K_{12}\frac{\partial\xi(1,\theta)}{\partial\theta}=Bi\xi(1,\theta);R_1\equiv1 \tag{13}$$

$$\xi(R_2,\theta)=\cos(\theta) \tag{14}$$

$$\frac{\partial\xi(R,0)}{\partial\theta}=\frac{\partial\xi(R,\pi)}{\partial\theta}=0 \tag{15}$$

The maximum value of the cross direction heat conduction coefficient, $K_{12}$, is limited according to the following Eq. (15):

$$k_{ii}k_{jj} - k_{ij}^2 > 0 \text{ for } i \neq j \tag{16}$$

For i=1 and j=2, and after dividing the equation by $(k_{11})^2$, equation (16) can be written in the following non-dimensional form:

$$K_{22} - K_{12}^2 > 0 \tag{17}$$

In order to better study the effect of the anisotropicity factor, $K_{12}$, it is convenient to normalize $K_{12}$ using $K_{22}$. The equation for the normalized non-dimensional cross direction conduction coefficient, $K^*_{12}$ can be written as follows:

$$0 \le K_{12}^* \le 1.0 \; ; \; K_{12}^* \equiv \frac{K_{12}}{\sqrt{K_{22}}} \tag{18}$$

The equal signs on both sides represent the limiting values of $K^*_{12}$.

## Numerical Procedure

The system of Eqs. (12-15) was solved using the finite difference method. All terms in Eq. (12) were discretized using second order accurate central difference formulas. The chain rule was used for the first term in Eq. (12). Thus the finite difference form of Eq. (12) become:

$$\frac{1}{R_i}\frac{\xi_{i+1,j} - \xi_{i-1,j}}{2\Delta R} + \frac{\xi_{i+1,j} - 2\xi_{i,j} + \xi_{i-1,j}}{(\Delta R)^2} + 2K_{12}\frac{1}{R_i}\frac{\xi_{i+1,j+1} - \xi_{i+1,j-1} - \xi_{i-1,j+1} + \xi_{i-1,j-1}}{4\Delta R\Delta\theta}$$
$$+ K_{22}\frac{1}{R_i^2}\frac{\xi_{i,j+1} - 2\xi_{i,j} + \xi_{i,j-1}}{(\Delta\theta)^2} = i\alpha\xi_{i,j} \tag{19}$$

The boundary condition on the cylinder inner surface was discretized using second order accurate forward difference formula for the radial term and second order accurate central difference formula for the tangential term. Thus the finite difference form of Eq. (13) was written as follows:

$$\frac{-\xi_{2j} + 4\xi_{1j} - 3\xi_{oj}}{2\Delta R} + K_{12}\frac{\xi_{oj+1} - \xi_{oj-1}}{2\Delta\theta} = Bi\,\xi_{oj} \tag{20}$$

At the inner radius, R=1.0, by definition, and i=0. The finite difference form of Eqs. (14) and (15) respectively, become

$$\xi_{N,j} = \cos(j^*\Delta\theta) \tag{21}$$

$$\xi_{i,-1} = \xi_{i,1} \; ; \; \xi_{i,m+1} = \xi_{i,m-1} \tag{22}$$

The system of algebraic Eqs. (19-22) was solved using the Gauss-Seidel explicit iterative

method [18]. The large size of the complex matrix generated by the finite difference method made more practical to use the Gauss-Seidel explicit iterative method than the analytical matrix algebra. The solution domain was divided into (n+1)* (m+1) equally spaced grid points in the radial and tangential directions, respectively, as shown in Fig. 2.

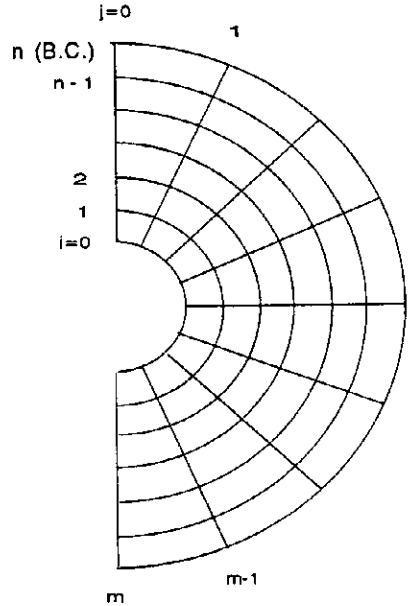


**Fig. 2. Schematic of the finite difference grid used**

In search of the optimal compromise between speed and accuracy, several grid sizes were tested. The number of grid points in the radial direction, N+1, was varied from 15 up to 120. The number of grid points in the tangential direction, M+1, was varied from 6 up to 50. The results reported in this paper are based on a 41*16 gird. The use of a finer grid size did not result in any noticeable change in the results, Fig. 3.

The iterative procedure was repeated until each of the cumulative absolute values of the real and imaginary errors became less than a predefined tolerance parameter, ε. After several test runs, the value of ε was set at $10^{-6}$. Smaller values of ε did not change the results of the numerical solution. Thus the convergence condition can be written as:

$$\sum_{n=0}^{40}\sum_{m=0}^{15}\left[\left|\mathrm{Re}[\xi_{n,m}^{new}]-\mathrm{Re}[\xi_{n,m}^{old}]\right|\right]<\varepsilon \qquad (23)$$

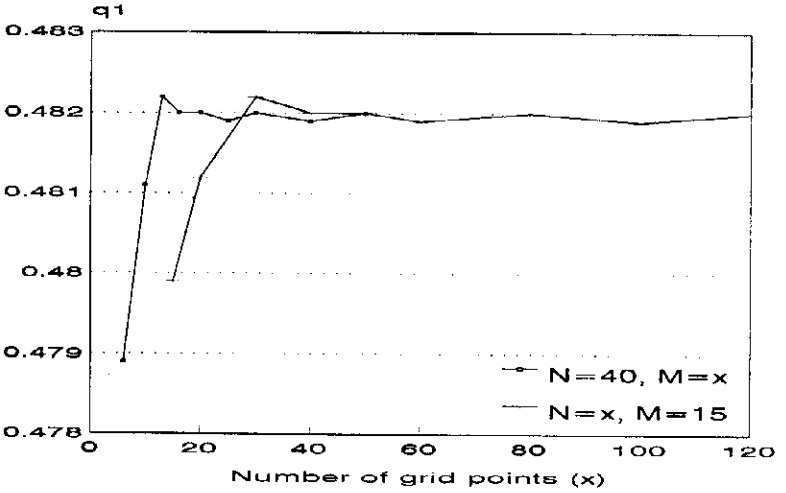


**Fig. 3. Change in maximum radial heat conduction to the cylinder inner wall as a function of grid size**

$$\sum_{n=0}^{40}\sum_{m=0}^{15}\left[\left|\mathrm{Im}[\xi_{n,m}^{new}]-\mathrm{Im}[\xi_{n,m}^{old}]\right|\right]<\varepsilon \qquad (24)$$

The final combination used for the remainder of this paper was a grid made from 41*16 points and a tolerance value of $10^{-6}$. The solution converged after 1200 to 1600 iterations. Higher $K^*_{12}$ values resulted in an increase in the number of iterations required for convergence.

## Results and Discussion

This section will report on the influence of the non-dimensional parameters on the periodic radial heat conduction in the cylinder. The parameters studied are: non-dimensional frequency ($\alpha$), non-dimensional outer radius ($R_2$), Biot number (Bi), the ratio of the tangential to the radial heat conduction coefficient, referred to herein as the orthotropicity factor ($K_{22}$), and the ratio of the cross directional to the tangential heat conduction coefficient, referred to herein as the anisotropicity factor ($K^*_{12}$). The results include the effect of each parameter on the maximum value of the non-dimensional radial periodic heat conduction to the cylinder inner and outer walls, $q_1$ and $q_2$ respectively, as well as the phase shift between $q_1$ referenced to $q_2$. The value of each parameter was varied separately over the range in which it exhibited a noticeable effect on the value of $q_1$. A reference value for each parameter was used for all cases except when the effect of the parameter was being investigated.

Since the main focus of this paper is the effect of anisotropicity, ten values of $K_{22}$ and five values of $K^*_{12}$ at each $K_{22}$ value were used while studying the effect of each of the other three parameters. The $K_{22}$ values used were 0.2, 0.5, 0.7, 1.0, 2.0, 5.0, 10.0, 20.0,

50.0 and 100.0. Due to space constraints selective results will be included herein. These values span the range of $K_{22}$ values studied and give a clear idea as to the general trend for the rest of the data. The five $K^*_{12}$ values used were 0.0, 0.25, 0.5, 0.75, 1.0. The value of $K^*_{12} = 0.0$ represents the orthotropic case and is included for comparison with the analytical solution [14] for the case of $K_{22} = 2.0$. The comparison served to validate the accuracy of the numerical solution. The reference values for the other three parameters were: $\alpha = 3.0$, Bi = 0.7, and $R_2 = 1.5$. These values were chosen a priori in order to facilitate direct comparison with the analytical results reported [14] and have no other special meaning.

Figure 4 shows the change of the maximum non-dimensional radial heat conduction at the inner radius, $q_1$, across the effective range of the non-dimensional frequency ($\alpha$). The figure includes two $K_{22}$ values, 2.0 and 10.0. Figure 4.a also includes the analytical solution for the case of $K^*_{12} = 0.0$. This figure shows a good agreement between the numerical and analytical results. For the orthotropic curves, $K^*_{12} = 0.0$, the value of $q_1$ decreased as $K_{22}$ increased. This is expected as a higher $K_{22}$ value indicates a lower relative tangential to radial heat conduction resistance. Thus more of the heat energy input at the outer wall is conducted in the tangential direction. For the same values of $K_{22}$, an increase in the value of $K^*_{12}$ results in an increase in $q_1$. This indicated that part of the heat energy conducted in the tangential direction is transferred to the radial direction through the effect of the cross direction conduction coefficient. The effect of $K^*_{12}$ on $q_1$ is minimal for low values of $K_{22}$. This is due to the fact that a small $K_{22}$ value would result in a small value of $K_{12}$. The change in $q_1$ became more significant as $K_{22}$ values increase. This can be seen clearly in the case of $K_{22} = 10.0$, Fig. 4.b. For all values of $K_{22}$, the slope of the $q_1$ versus a curve increased as the $K^*_{12}$ value increased. This trend became more apparent at higher values of $K_{22}$, Fig. 4.b.

Figure 5 shows the effect of $\alpha$ on the maximum non-dimensional radial heat conduction to the cylinder outer wall, $q_2$. Figure 5.a also includes the analytical solution for the case of $K^*_{12} = 0.0$. This figure shows a good agreement between the numerical and analytical results. Comparing the different orthotropic curves, $K^*_{12} = 0.0$, shows that as the $K_{22}$ value increased the value of $q_2$ increased. This is expected as a higher $K_{22}$ value would result in a lower overall heat conduction resistance. This is reflected as an increase in the heat energy conducted to the cylinder's outer wall. For the same $K_{22}$ value, an increase in the $K^*_{12}$ value resulted in an increase in $q_2$. Higher $K^*_{12}$ values result in lower overall radial heat conduction resistance and thus higher $q_2$ values. The effect of $K^*_{12}$ on $q_2$ was visible for all values of $K_{22}$, but became more evident at higher $K_{22}$ values, Fig. 5.b. For all $K_{22}$ values, the slope of $q_2$ versus $\alpha$ decreased as $K^*_{12}$ increased. For all values of $K_{22}$ in Fig. 5, an equal increase in $K^*_{12}$ resulted in an equal increase in $q_2$. For the same $K_{22}$ value, changing the $K^*_{12}$ value did not result in any noticeable change in the steady state value of $\alpha$. The steady state $\alpha$ is defined as the maximum $\alpha$ value below which the value of $q_2$ became insensitive to any further reduction in $\alpha$.

Figure 6 shows the effect of changing $\alpha$ on the phase shift between the maximum

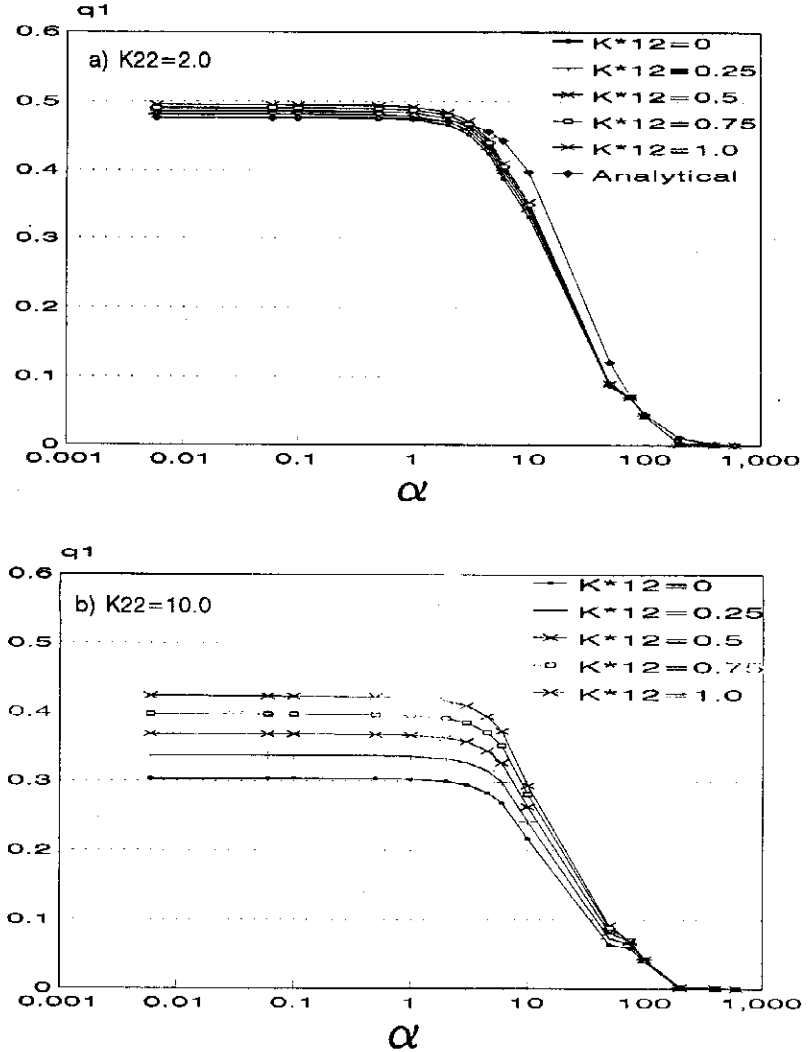


**Fig. 4. Effect of non-dimensional frequency on maximum radial heat conduction to the cylinder inner wall.**

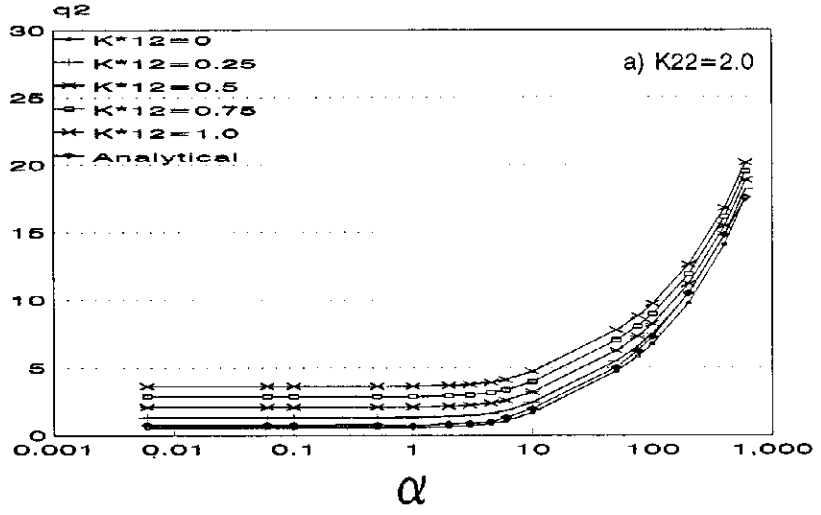


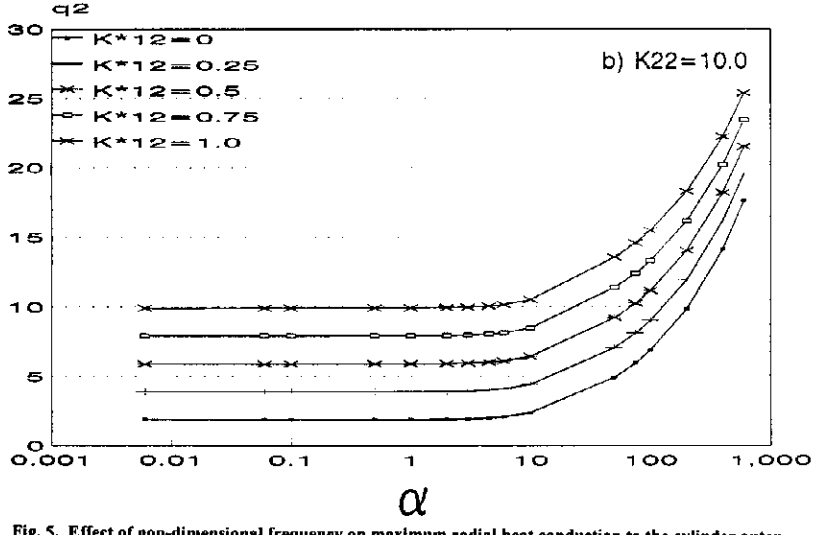


**Fig. 5. Effect of non-dimensional frequency on maximum radial heat conduction to the cylinder outer wall.**

radial heat conduction at the cylinder inner radius, $q_1$, reference to the maximum radial heat conduction at the cylinder outer radius, $q_2$. Fig. 6.a includes the analytical solution for the case of $K_{22} = 2.0$ and $K^*_{12} = 0.0$. The sharp phase transitions seen are due to the fact that the phase value is limited between $-\pi$ and $+\pi$. When the value of the phase shift becomes smaller than $-\pi$, the phase is modified by adding $2\pi$ to it. This results in a sharp increase in phase. There is an excellent agreement between the analytical and numerical curves. Actually, the two curves collapse and cannot be distinguished over the entire range of $\alpha$ except at the last $\alpha$ value, $\alpha = 600$. The difference at this value could be due to the low $q_1$ value at this high $\alpha$ point and/or the error in the analytical solution that starts at high $\alpha$ values [14]. At low values of $\alpha < 0.1$, the effect of $K^*_{12}$ was to change the phase from approximately zero for the orthotropic case, $K^*_{12} = 0.0$, to $-\pi$ for all other anisotropic cases, $K^*_{12} \neq 0.0$.

There was no noticeable difference among the four anisotropic curves in the range $\alpha < 0.1$. For $\alpha > 0.1$ the phase curves corresponding to the lowest anisotropic case, $K^*_{12} = 0.25$, started to increase as the orthotropic phase curve started to decrease until both curves met. The rate at which the $K^*_{12} = 0.25$ curve increased to the point at which it met the orthotropic curve depended strongly on the value of $K_{22}$. This can be seen clearly when comparing Figs. 6.a and 6.b. The higher the $K_{22}$ value the lower the change in the anisotropic phase curve and the higher the $\alpha$ value at which the two curves met. For the same $K_{22}$ values, the higher the $K^*_{12}$ value the less sensitive the phase curve became to the effect of changing $\alpha$. High $K_{12}$ values which result from the combination of high $K^*_{12}$ and/or $K_{22}$ values, Eq. (18), tended to stabilize the phase across a wider range of $\alpha$. The phase shift indicates the speed at which the heat wave travels across the cylinder. Thus the heat wave speed became relatively constant at high $K_{12}$ values.

Figure 7 shows the effect of Biot number (Bi) on $q_1$. Although not clear in Fig. 7.a, the colored output on computer screen of the figure showed that the analytical and numerical orthotropic $q_1$ versus Bi curves collapsed over the entire range of Bi. A colored figure could not be included with this paper for technical considerations. For all cases, as Bi increased, $q_1$ increased up to a maximum value beyond which $q_1$ remained constant. This is expected as higher Bi values result in lower radial heat conduction resistance. For a given $K_{22}$ value, $q_1$ value increased as $K^*_{12}$ increased, but the rate of change of $q_1$ with respect to Bi decreased with increasing $K^*_{12}$ value. The change in $q_1$ was minimal for low $K_{22}$ values, $K_{22} = 2.0$, but became more evident at higher $K_{22}$ values, $K_{22} = 10.0$. This is expected since a higher $K_{22}$ value would result in higher $K_{12}$ values. For $K^*_{12} = 1.0$, the curves of $q_1$ versus Bi were similar, in both magnitude and slope, regardless of the value of $K_{22}$. For a given value of $K_{22}$, the slope of the $q_1$ versus Bi curve increased as $K^*_{12}$ increased. This was more apparent in the case of $K_{22} = 10.0$. The effective Bi range remained constant for all $K_{22}$ and $K^*_{12}$ values.

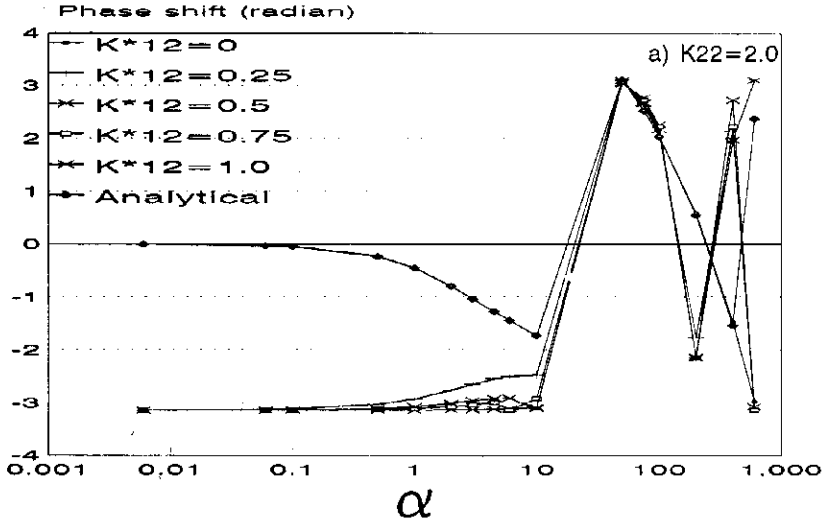


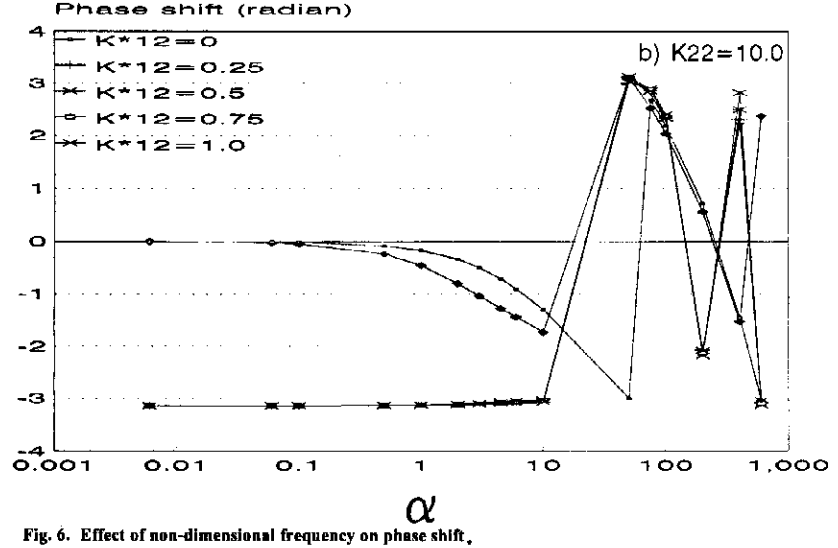


**Fig. 6. Effect of non-dimensional frequency on phase shift.**

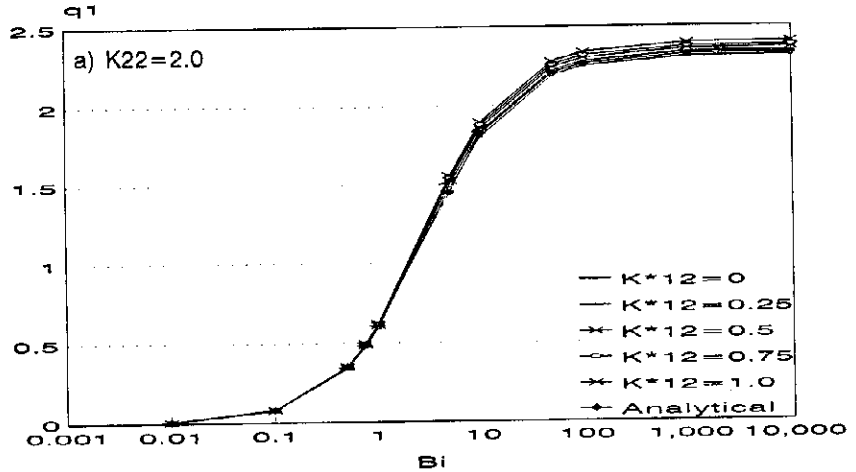


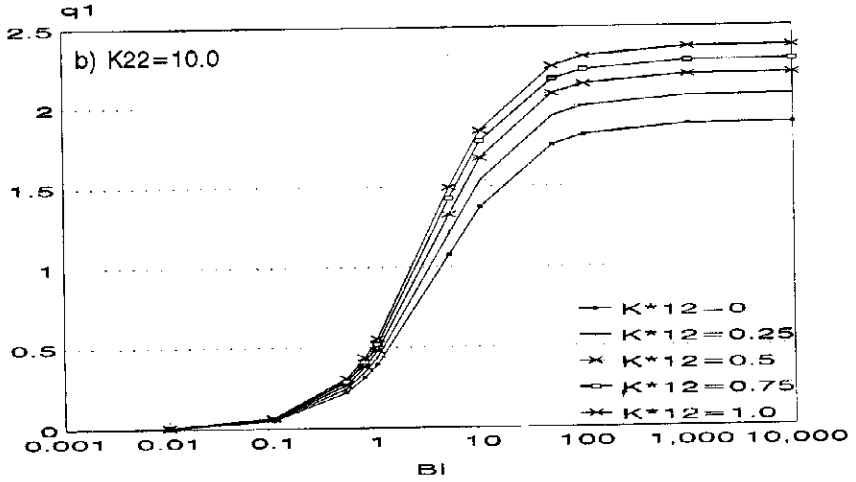


**Fig. 7. Effect of Biot number on maximum radial heat conduction to the cylinder inner wall.**

Figure 8 shows the effect of cylinder outer radius, $R_2$, on $q_1$. Logarithmic scale is used for the x-axis in the figure, i.e. $R_2$. Figure 8.a shows a good agreement between the analytical and numerical orthotropic solutions. The only exception is around $R_2 = 2.0$. The effect of anisotropicity is not apparent in Fig. 8.a. This could be attributed to the low values of $K_{22}$. Higher $K^*_{12}$ values resulted in higher $q_1$ values at the same $R_2$. The $q_1$ curves corresponding to higher $K^*_{12}$ values exhibited more gradual decline at higher $R_2$ values. This effect became more visible as $K_{22}$ value increased, Figs. 9.c and 9.d. In all figures, the difference in $q_1$ due to $K^*_{12}$ is limited to the $R_2$ range of 1.2 to 5.0. At the low end of the $R_2$ range the $q_1$ value is approximately the same irrespective of the $K_{22}$ and $K^*_{12}$ values.

Figure 9 shows the effect of $R_2$ on $q_2$. Figure 9.b includes the analytical solution of $q_2$ versus $R_2$ at $K_{22} = 2.0$. There is good agreement between the analytical and numerical values of $q_2$ over the entire range of $R_2$. For all $K_{22}$ values, higher $K^*_{12}$ values resulted in higher $q_2$ values. This effect is clear for all values of $K_{22}$ and continues even at the asymptotic value of $q_2$. In the range $R_2 < 2.0$, the behavior of $q_2$ versus $R_2$ is different among the four $K_{22}$ values specially at low $K^*_{12}$ values. Fig. 9.a, shows that $q_2$ tends to decrease then increase in the range of $R_2 < 2.0$. This can be seen to different extents for all values of $K^*_{12}$. While on the other extreme, Fig. 9.d at $K_{22} = 100.0$, $q_2$ tends to increase then decreases in the range of $R_2 < 2.0$. Again, this behavior is more evident at lower $K^*_{12}$ values. Comparing the different curves in Fig. 9, a higher value of $K_{22}$ results in higher $q_2$ values. This is attributed mainly to the reduction in the cylinder overall heat conduction resistance.

Figures 10.a, 10.b and 10.c show the effect of $K_{22}$ on $q_1$, $q_2$ and phase shift, respectively. Each figure also contains the curves of the analytical and numerical orthotropic solutions. The agreement between the two curves is excellent in all three figures across the range of $K_{22}$. The only exception is the phase shift at high values of $K_{22}$, Fig. 10.c. The cause of this has been mentioned when discussing Figure 6.a. Figure 10.a shows that as $K^*_{12}$ increases, $q_1$ increases. The effect of $K^*_{12}$ is not clear at low values of $K_{22}$, which results in lower $K_{12}$ values, but becomes more significant as $K_{22}$ increases. Higher $K^*_{12}$ values tend to stabilize the change in $q_1$ over the range of $K_{22}$. There are no surprises in Figure 10.b where higher $K_{22}$ values resulted in higher $q_2$ value. Also a higher $K^*_{12}$ values resulted in higher $q_2$ values. The effect of $K^*_{12}$ increased as $K_{22}$ value increased due to the resulting higher $K_{12}$ value. Figure 10.c shows the stabilizing effect of $K_{12}$ on the phase shift. As $K_{22}$ and $K^*_{12}$ increased, the phase shift tended to remain constant at around -3 radians. The closest anisotropic curve to the orthotropic curve was that of $K^*_{12} = 0.25$ at the low end of the $K_{22}$ range. This is expected as the $K_{12}$ value at this combination is small.

Figure 11 shows the tangential variation in the local radial heat conduction at the cylinder inner wall, $q_{L1}$, at the reference conditions of $\alpha$, Bi, and $R_2$. The comparison between the orthotropic analytical and numerical solutions in Fig. 11.b shows excellent agreement between the two curves. As $K^*_{12}$ increases, the $q_{L1}$ curves start to deviate from the orthotropic cosine curve. This deviation includes a reduction in the average value of the $q_{L1}$ as well as a lower magnitude change across the cylinder tangential direction. This

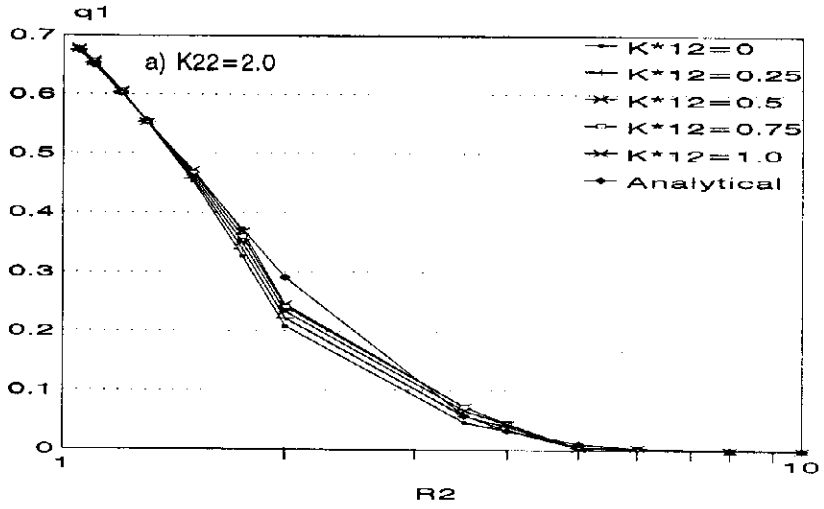


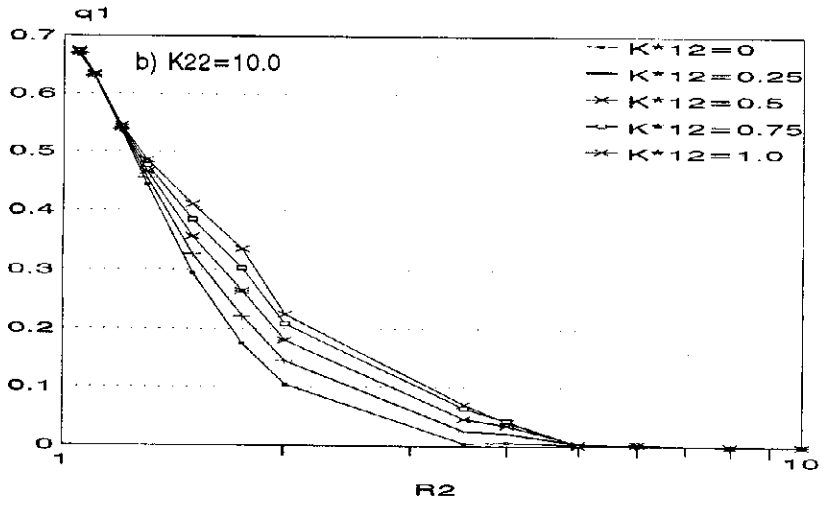


**Fig. 8. Effect of cylinder outer to inner radius ratio on maximum radial heat conduction to the cylinder inner wall.**

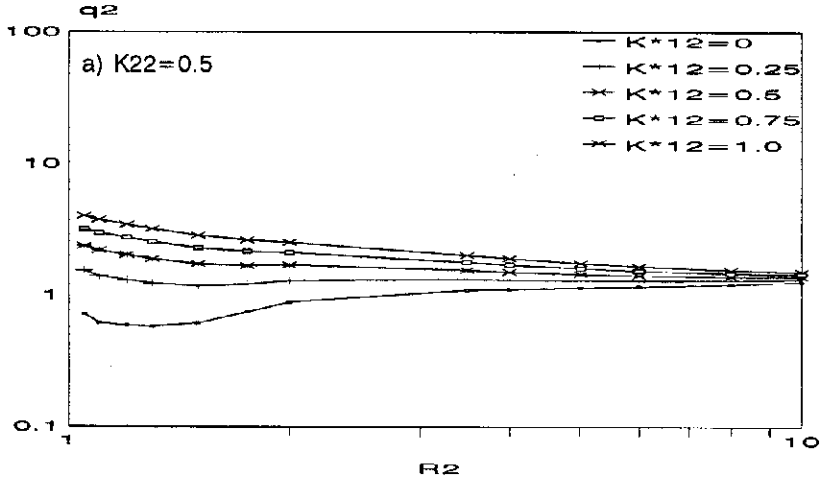


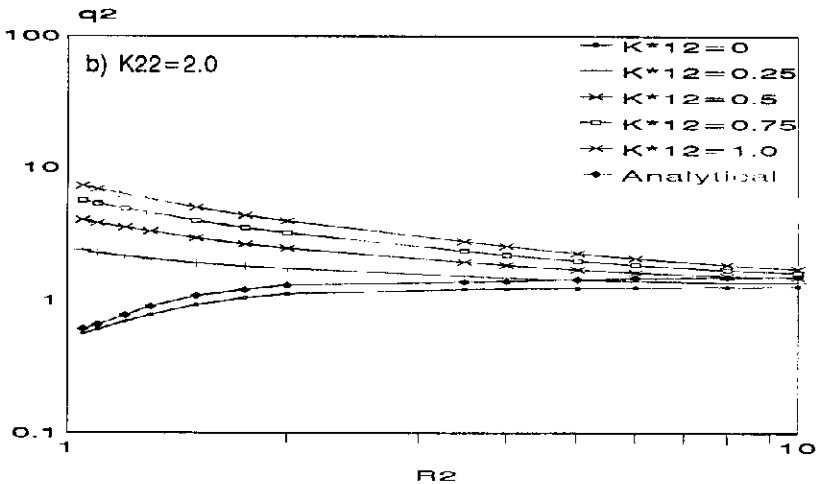


**Fig. 9. Effect of cylinder outer to inner radius ratio on maximum radial heat conduction to the cylinder outer wall (cont.).**

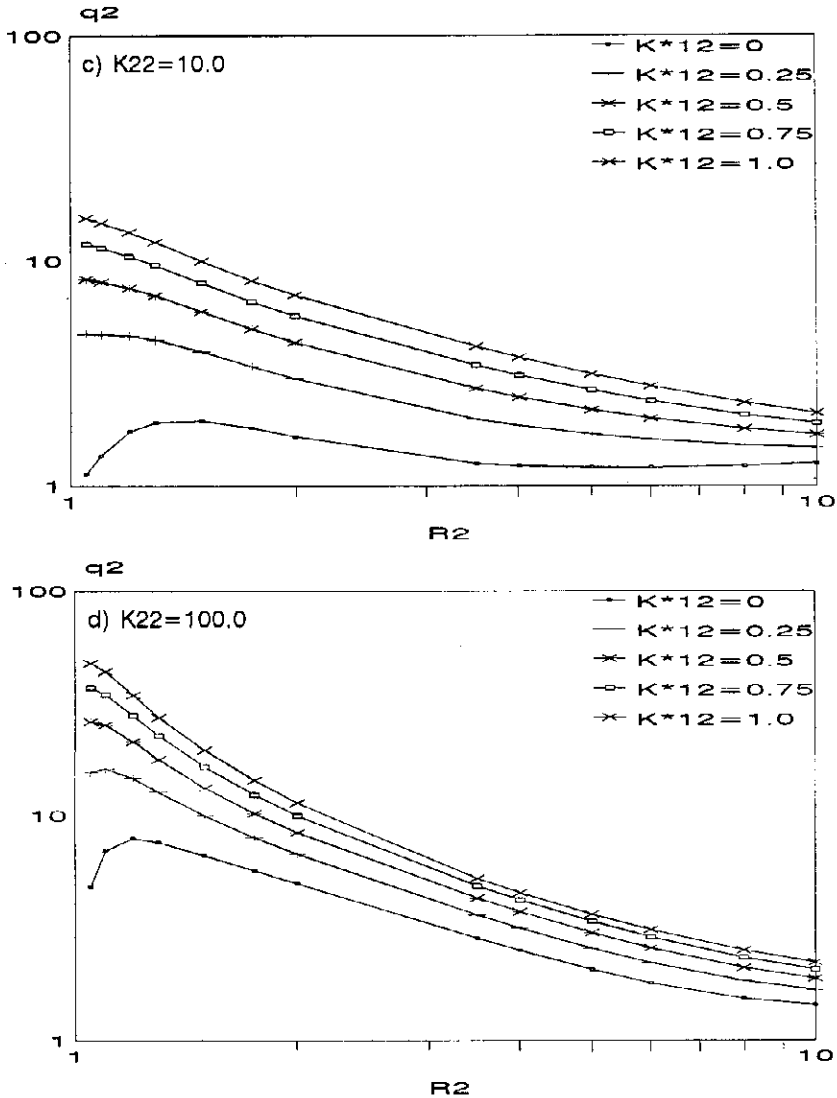


**Fig. 9. Effect of cylinder outer to inner radius ratio on maximum radial heat conduction to the cylinder outer wall.**

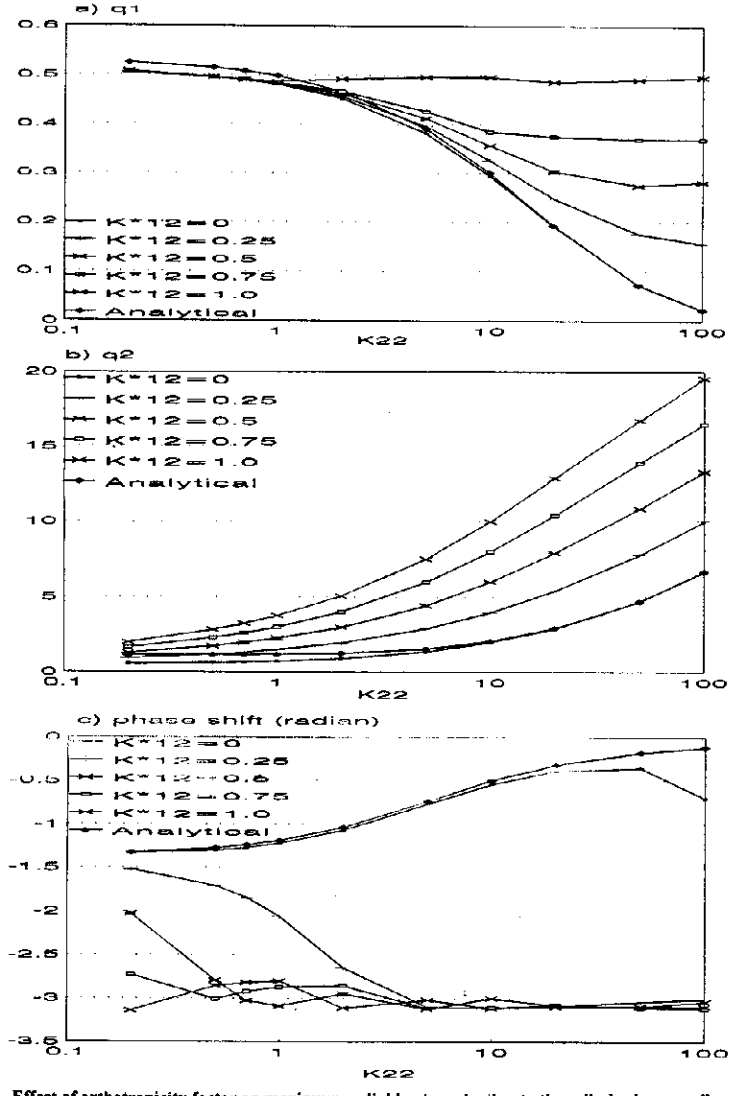


**Fig. 10. Effect of orthotropicity factor on maximum radial heat conduction to the cylinder inner wall, maximum radial heat conduction to cylinder outer wall, and phase shift.**

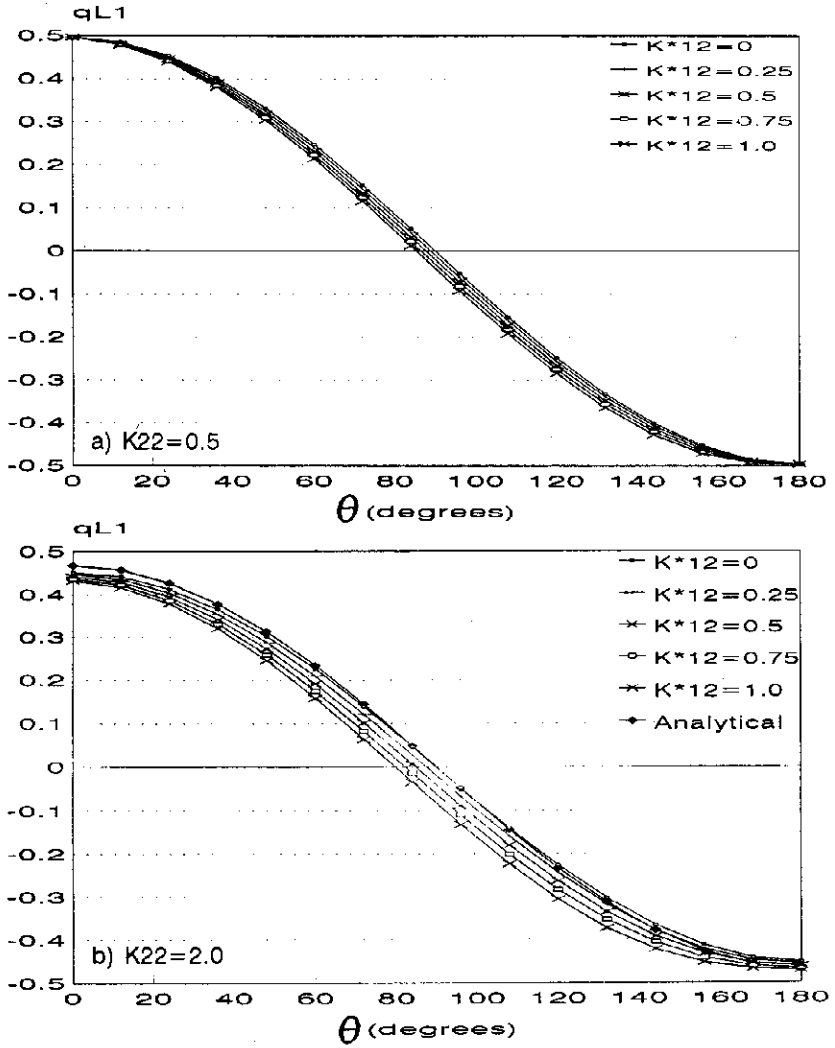


**Fig. 11. The tangential variation of local non-dimensional radial heat conduction at the cylinder inner wall (cont.).**

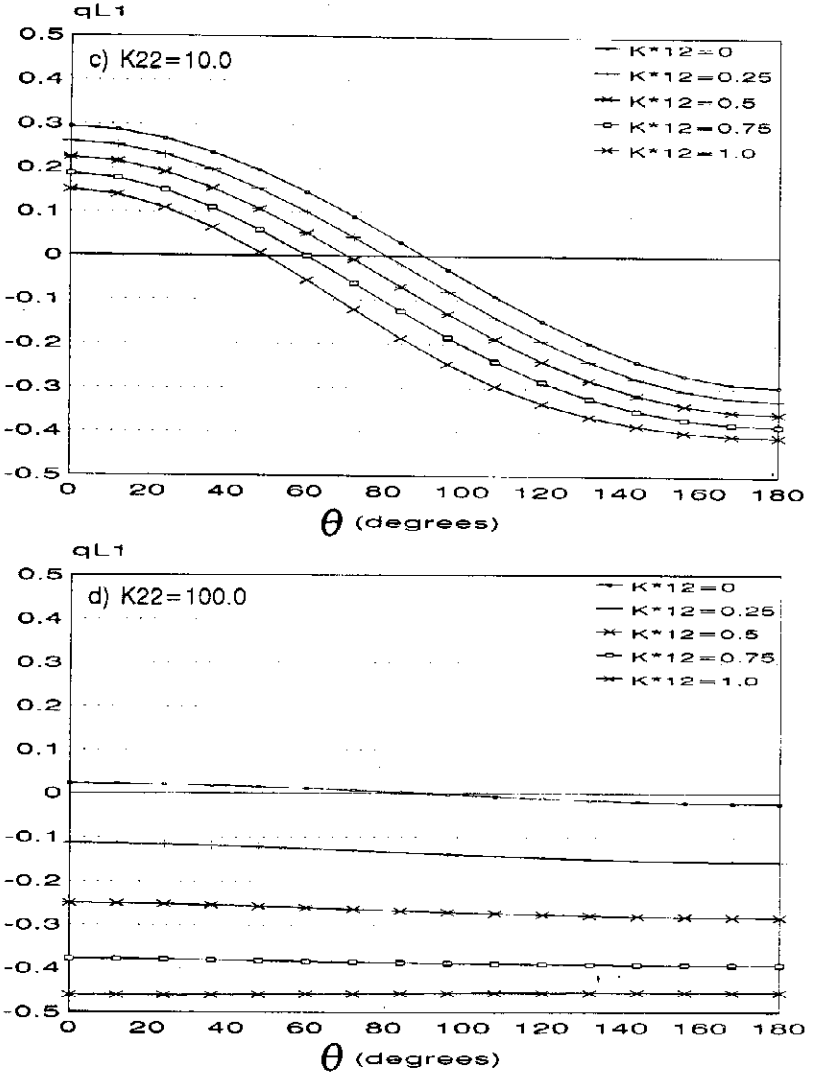


**Fig. 11. The tangential variation of local non-dimensional radial heat conduction at the cylindler inner wall.**

deviation includes a reduction in the average value of the $q_{L1}$ as well as a lower magnitude change across the cylinder tangential direction. This deviation increases as $K_{22}$ increases mainly due to the increase in the $K_{12}$ value. Figure 11.d shows the extent to which the value of $K^*_{12}$ can affect the $q_{L1}$ curves. Interestingly, the curve of $K_{22} = 100.0$ and $K^*_{12} = 1.0$ shows an almost constant yet definitely inverted cosine $q_{L1}$ curve.

Figure 12 shows the tangential variation in the local radial heat conduction at the cylinder outer wall, $q_{L2}$, at the reference conditions of $\alpha$, Bi, and $R_2$. Figure 12.b shows the excellent agreement between the numerical and analytical orthotropic $q_{L2}$ curves. The effect of $K^*_{12}$ on the $q_{L2}$ curves is most visible at $\theta$ values of 0 and 180 degrees. At these points, the anisotropic curves deviate significantly from the cosine curve of the orthotropic solution. For the orthotropic case, the plane of symmetry passing through $\theta = 0$ and 180 degrees did not influence the $q_{L2}$ values at those points. In the anisotropic cases, the coupling between the radial and tangential conduction terms resulted in significant deviation in the $q_{L2}$ values at the same points. The effect of this boundary condition penetrated further into the tangential direction as $K_{22}$ value increased. This could be seen clearly in Fig. 12.d, $K_{22} = 100.0$. The effect of $K^*_{12}$ was to increase the magnitude of $q_{L2}$ significantly around the plane of symmetry, specially at $\theta = 180$ degrees. This effect increased as $K_{12}$ increased.

Figure 13 shows the tangential variation in the local phase shift at the reference conditions of $\alpha$, Bi, and $R_2$. Figure 13.b shows the excellent agreement between the numerical and analytical orthotropic phase shift curves. The anisotropic phase shift curves deviated from the constant phase curve of the orthotropic curves. At the low $K_{22}$ value of 0.5, the deivation was concentrated in a small region, $\theta = 85$ to 120 degrees in figure 13.a. The deviation increased to cover most of the tangential range at $K_{22} = 100.0$, Fig. 13.d. In each case, higher $K^*_{12}$ values resulted in greater deviation from the orthotropic curves.

## Conclusions

The problem of heat conduction in an anisotropic cylinder subjected to an asymmetric and periodic temperature distribution on its outer wall was solved numerically. The non-dimensional form of the equation showed that the heat conduction across the cylinder as dependent on five parameters: non-dimensional frequency ($\alpha$), Biot number (Bi), nondimensional outer radius ($R_2$), orthotropicity factor ($K_{22}$), and normalized anisotropicity factory ($K^*_{12}$). The study reports on the effect of each parameter on the maximum radial heat conduction to the cylinder inner and outer walls, $q_1$ and $q_2$, and the phase shift between $q_1$ and $q_2$. The results showed that the magnitude of the radial heat conducted to the inner and outer walls can be altered to different degrees based on the combination of the aforementioned parameters. A cylinder made from a material with a high $K_{22}$ and low $K_{12}$ values would exhibit excellent insulation characteristics subjected to an asymmetric and cyclic temperature distribution on the cylinder outer wall. Such a cylinder could be made using circumferentially wound high thermal conductivity fibers. While a cylinder with a high $K_{22}$ and $K_{12}$ values would exhibit high radial heat conduction characteristics

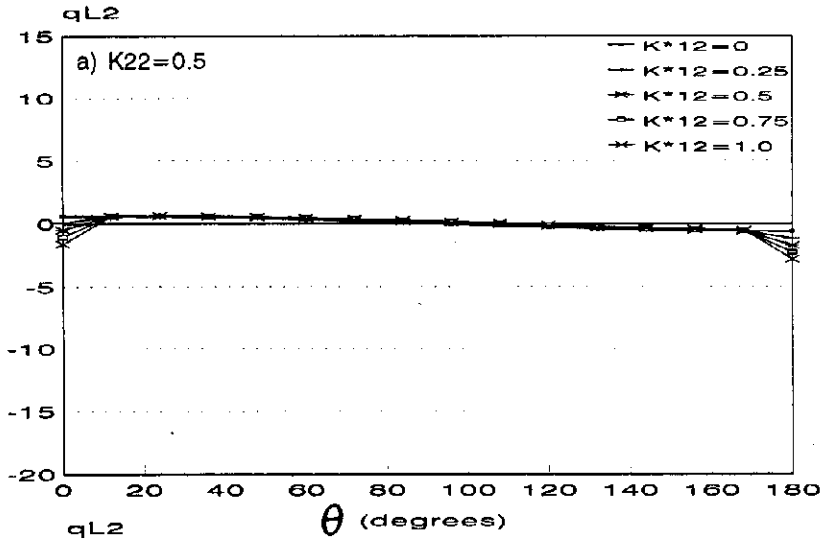


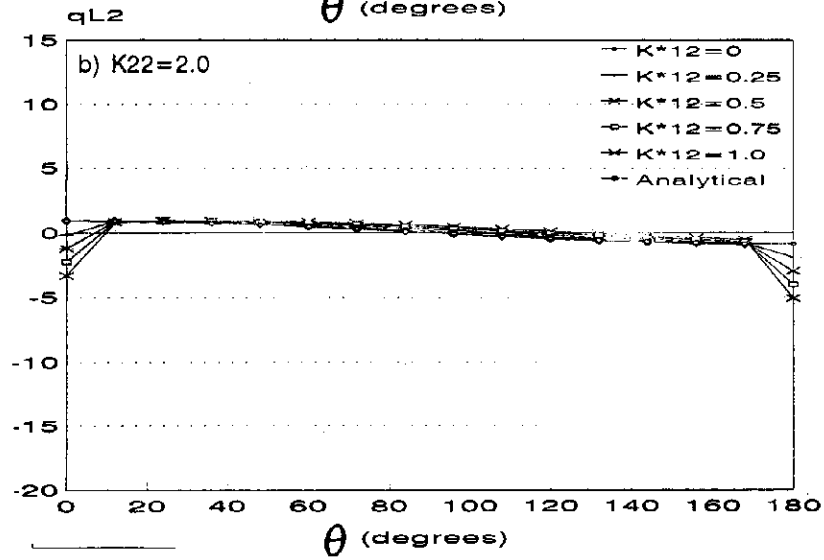


**Fig. 12. The tangential variation of local non-dimensional radial heat conduction at the cylinder outer wall (cont.),**

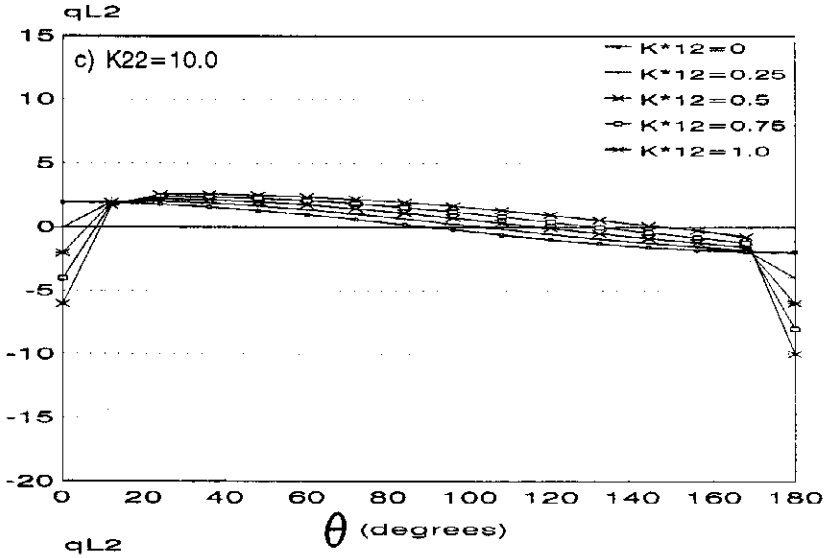


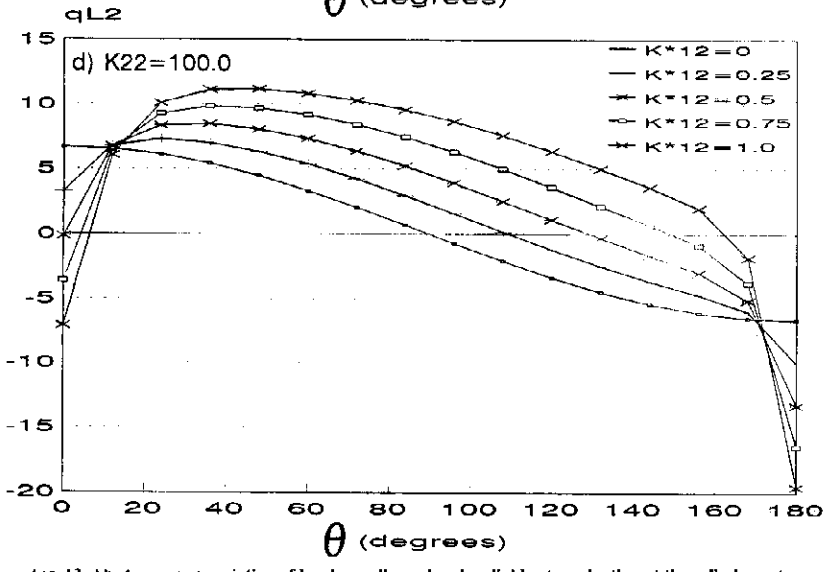


Fig. 12. The tangential variation of local non-dimensional radial heat conduction at the cylinder outer wall.

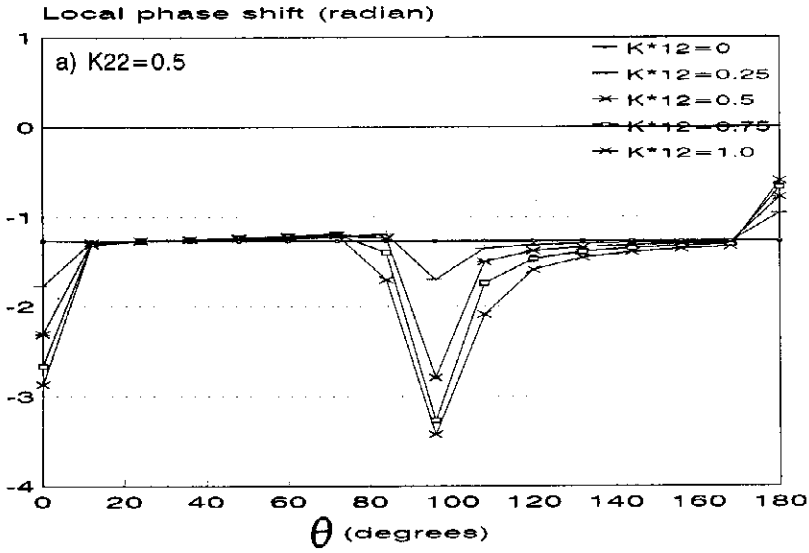


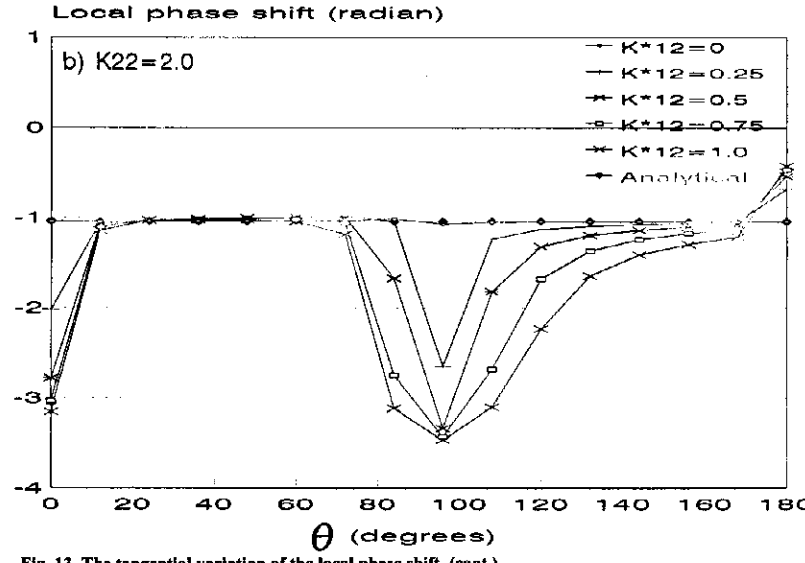


**Fig. 13. The tangential variation of the local phase shift (cont.),**

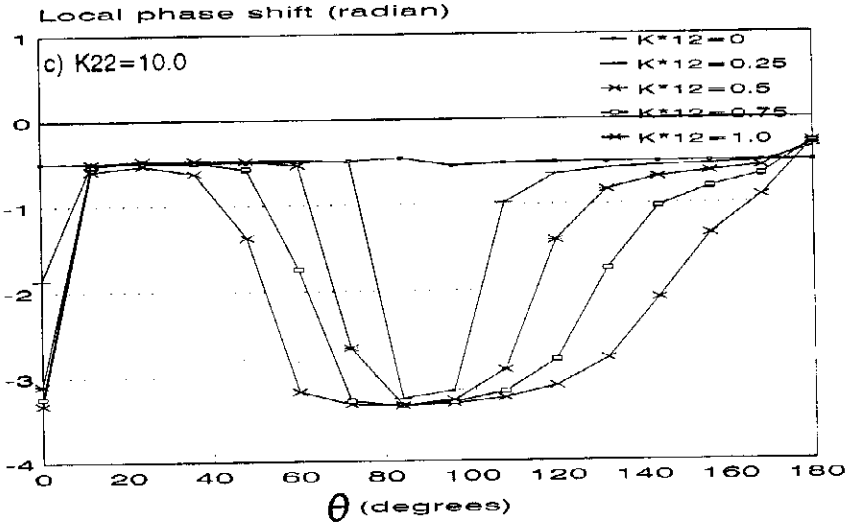


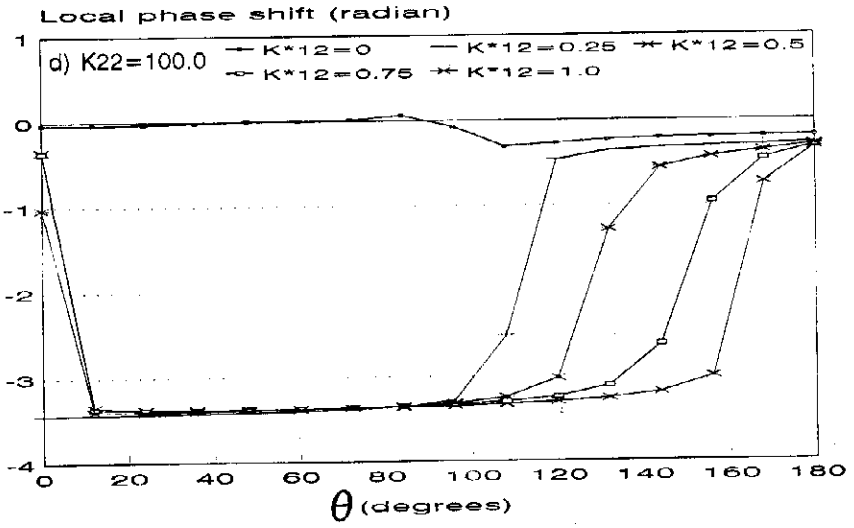


**Fig. 13. The tangential variation of the local phase shift.**

when subjected to an asymmetric and cyclic temperature distribution on the cylinder outer wall.

## References


[1] Coalesce, W.A. *A Textbook in Crystal Physics.* London: Cambridge University Press, 1938.

[2] Nye, J.F. *Physical Properties of Crystals.* London: Clarendon Press, 1957.

[3] Carslaw, H.A. and Jaeger, J.C. *Conduction of Heat in Solids.* London: Clarendon Press, 1957.

[4] Chang, Y.P. and Tsou, R.C.H. "Heat Conduction in an Anisotropic Medium Homogeneous in Cylindrical Regions - Unsteady State." *Journal of Heat Transfer.* 99, No.2 (1977), 41-46.

[5] Boley, B.A. and Weiner, J.H. *Theory of Thermal Stress.* New York: Wiley, 1960.

[6] Hyer, M.W., Coper, D.E. and Cohen, D. "Stresses and Deformations in Cross-Ply Composite Tubes Subjected to a Uniform Temperature Change". *Journal of Thermal Stresses*, 9, No. 9 (1986), 97-117.

[7] Thangjithem, S. and Choi, H.J. "Thermal Stresses in Asymmetrically Heat Radiated Tubes." *Journal of Applied Mechanics,* 58, No. 12 (1991), 1021-1027.

[8] Xianghou, Z. "Steady-State Tempeatures in an Anisotropic Strip." *Journal of Heat Transfer*, 112, No. 2 (1990), 16-20.

[9] Chao, C.K. and Chang, R.C. "Steady-State Heat Conduction Problem of the Interface Crack Between Dissimilar Anisotropic Media." *International Journal of Heat and Mass Transfer.*, 36, No.8 (1993), 2021-2026.

[10] Zibdeh, H.S. and Farran, J.M. "Stress Analysis in Composite Hollow Cylinders due to an Asymmetric Temperature Distribution. *Journal of Pressure Vessel Technology.* 117, No. 2 (1995), 59-65.

[11] Fett, T. "Temperature Distribution and Thermal Stresses in Asymmetrically Heat Radiated Tubes." *Journal of Applied Mechanics,* 53, No.3 (1986), 116-120.

[12] Kardomateas, G.A. "Transient Thermal Stresses in Cylindrically Orthotropic Composite Tubes." *Journal of Applied Mechanics,* 56, No. 6 (1989), 411-417.

[13] Chen, L.S. and Chu, H.S. "Transient Thermal Stresses of a Composite Hollow Cylinder Heated by a Moving Line Source." *Computers & Structures,* 33, No. 5 (1989), 1205-1214.

[14] Kardomateas, G.A. "The Initial Phase of Transient Thermal Stresses due to General Boundary Thermal Loads in Orthotropic Hollow Cylinders." *Journal of Applied Mechanics*, 57, No. 9 (1990), 719-724.

[15] Ootao, Y., Tanigawa, Y. and Fukuda, T. "Axisymmetric Transient Thermal Stress Analysis of a Multilayered Composite Hollow Cylinder." *Journal of Thermal Stresses*, 14, No. 14 (1991), 201-213.

[16] Abu-Hijleh, B. "Enhanced Thermal Insulation Characteristics of a Cylinder Using Orthotropic Material." *The International Journal of Energy,* 22, No.5 (1997), 471-476.

[17] Ozisik, M.N. *Heat Conduction.* New York: John Wiley and Sons, 1980.

[18] Gerald, C.F. and Wheatley, P.O. *Applied Numerical Analysis.* New York: Addison Wesley, 1984.

# حلّ عددي لانتقال الحرارة في إسطوانة ذات معاملات انتقال حرارة غير متماثلة خاضعة لتوزيع حراري دوري و غير متماثل

بسام عبد الكريم أبو حجلة

*قسم الهندسة الميكانيكية ، جامعة العلوم و التكنولوجيا الأردنية ، ص . ب . ٣٠٣٠ ، إربد ٢٢١١٠ ، الأردن*

( استُلم في ١٩٩٥/١٠/٣٠م ؛ وقُبل للنشر في ١٩٩٦/٩/٢٩م )

**ملخص البحث** . توضّح هذه الورقة الحلّ العددي لانتقال الحرارة في إسطوانة ثنائيّة الأبعاد ذات معاملات انتقال حرارة غير متماثلة خاضعة لتوزيع حراري دوري وغير متماثل على السطح الخارجي للإسطوانة . أظهر تحليل الوحدات أنّ عمليّة انتقال الحرارة عبر الإسطوانة تعتمد على قيمة خمس مجموعات عديمة الوحدات هي : الذبذبة النسبيّة ، السماكة النسبيّة ، معامل (البيوت) ، معامل التوصيل الحراري النسبي في الاتّجاه المماسي ومعامل التوصيل النسبي الرابط بين الاتجاهين الشعاعي والمماسي . تفصّل الدراسة تأثير كل من هذه المجموعات على كميّة الحرارة الواصلة للجدارين الداخلي والخارجي للإسطوانة بالإضافة إلى إزاحة الطور بين الجدارين . تبعًا لقيم المجموعات المختلفة فإنّ مقدار و / أو إزاحة الطور لانتقال الحرارة في إسطوانة ذات معاملات انتقال حرارة غير متماثلة تختلف كثيرًا مقارنة مع مثيلاتها في إسطوانة ذات معاملات انتقال حرارة متماثلة تحت تأثير توزيع حراري دوري وغير متماثل على السطح الخارجي للإسطوانة .